IIETA International Information and Engineering Technology Association
Advancing the World of Information and Engineering

Traitement du Signal
Vol. 41, No. 4, August, 2024, pp. 2057-2067
Journal homepage: http://iieta.org/journals/ts

Design and Analysis of a Compact 4-Port MIMO Antenna for Improved Isolation and 5G (n78/n77/n48) Performance

Manumula Srinubabu*, Nuthakki Venkata Rajasekhar

School of Electronics Engineering, VIT-AP University, Amaravati 522237, India

Corresponding Author Email: srinubabu.21phd7112@vitap.ac.in

https://doi.org/10.18280/ts.410434

Received: 1 August 2023
Revised: 22 January 2024
Accepted: 8 March 2024
Available online: 31 August 2024

Keywords:
MIMO antenna, modified ground, decoupling, Isolation, efficiency, diversity parameters, 5G-NR n78/n77/n48 bands

ABSTRACT

This paper describes the compact design of a 4-port MIMO (multi-input, multi-output) antenna with enhanced diversity parameters for the n78/77/48 5G band. The proposed 4-port MIMO antenna design consists of a symmetrical two-pair monopole antenna placed closely (less than space diversity of $\lambda_{max}/2$). The MIMO antenna design incorporates Rogers RO3003 substrates with a ε_r of 3.2. The antenna size is compact, with dimensions of 78×64.5×1.6 mm^3 with enhanced isolation and diversity parameters. The T-shaped stub is etched from the ground and incorporated with grounding branching in the middle of the ground plane, which enhances the bandwidth, gain, and isolation. Moreover, placing a horizontal or vertical decoupling element between the two sets of antennas obstructs the reverse current path and reduces the S_{21}. The proposed antenna has an envelope correlation coefficient (ECC) of 0.00789, a diversity gain (D.G.) of 9.96 dB, a total effective reflection coefficient (TARC) of < -10 dB, a mean effective gain (MEG) of 0.01 dB, a channel capacity loss (CCL) of 0.24 bps/Hz, a peak gain of 4.4 dBi, and a radiation efficiency of 98.85% across the specified range, respectively. In addition, S_{21} is -22 dB across the bands. Further, the suggested antenna also has the advantages of compact size and better diversity parameters, which ensure its compatibility with modern n78/77/48 band 5G systems, Wi-Max bands, and V2V applications.

1. INTRODUCTION

The progression of fifth-generation (5G) wireless technology is swift, providing enhanced data rates, minimal latency, enhanced bandwidth, and improved connectivity [1-4]. To support these advanced features, the 5G system employs a new radio spectrum, functioning within frequency range 1 (FR-1, sub-6 GHz) and frequency range 2 (FR-2, the mm-wave band). N78 is one of the many sub-bands in the FR-1 5G NR spectrum. It employs an orthogonal orientation in its construction and operates as a WiMax band from 3.3 to 3.8 GHz [5-8]. The N78 band is likely to have a significant impact on the rollout of 5G networks. Multiple-input, multiple-output (MIMO) antennas become very important in 5G communication design in cities, especially where the short range and poor coverage of high-frequency bands make real-time use cases difficult [3, 9-12]. MIMO antennas play a pivotal role in enhancing the data rates and signal quality for 5G networks. By employing multiple antennas on both the transmitter and receiver sides, MIMO technology enhances the spectrum efficiency of wireless systems. But mutual coupling between antenna elements are a big problem in MIMO systems [1, 2, 13]. The antennas need to be well separated from each other to prevent interference and cross-talk between channels. In the real world of microstrip antennas, there persists dissatisfaction within the electromagnetic community regarding size reduction and the need for bandwidth enhancement. Hence, the design of a compact MIMO antenna becomes imperative for achieving optimal system performance. This paper introduces a compact, four-port MIMO antenna tailored for improved diversity, performance, and effective isolation in the N78 5G bands. The antenna is specifically crafted to operate within the frequency range of 3.3 to 3.8 GHz [2, 4, 14-17]. which is a critical frequency band for 5G communication. The diversity approach [18-20] is one of several strategies used to increase isolation. Along with these, there are metamaterials, decoupling elements (DE), electromagnetic band gaps (EBG), defective ground structures (DGS) [21], and ways to separate MPS radiators. Defected or modified ground structure (MGS) [21-23], parasitic parts [2, 24], neutralization boundary [2, 25], electromagnetic band gap design [2, 26, 27] and decoupling structures (DS) [2, 7, 8, 27-32] are also imprinted in MIMO antennas for enhancing bandwidth and isolation.

The simulation results indicate the effectiveness of the proposed antenna design, showcasing favorable impedance matching, improved isolation, better diversity performance, and consistent radiation patterns for the n78/77/48 5G band. The following sections provide a detailed exploration of the antenna design, methodology, simulated and experimental outcomes, and concluding remarks on the proposed antenna.

2. ANTENNA DESIGN AND METHODOLOGY

This section examines the complete evolution of the finalized antenna's design and performance in various scenarios. The following segments offer a thorough and systematic explanation of the design approach employed for the antenna. A single-monopole antenna is designed with DGS techniques for enhancing bandwidth and good impedance matching. 2-port MIMO antennas implemented different techniques (mirroring techniques, decoupling elements, and grounding branches) for isolation enhancement to reduce mutual coupling between the antennas for better antenna design. The proposed 4-port MIMO antenna incorporated another decoupling element between the 2×1 configuration for enhanced isolation for the required operating band (n77, 78, and 48 bands).

2.1 Single monopole antenna design evolution

This section describes the evolution of antennas over time and their performance in different situations. The following segments offer a thorough and systematic explanation of the design approach employed for the antenna. Figure 1 depicts the single monopole antenna step-by-step evolution with microstrip feeding, which is formed by a triangular cut etched from a rectangular patch antenna having dimensions of 34×35×1.6mm^3 and a loss tangent factor of 0.0013, which is referred to as Ant._1.

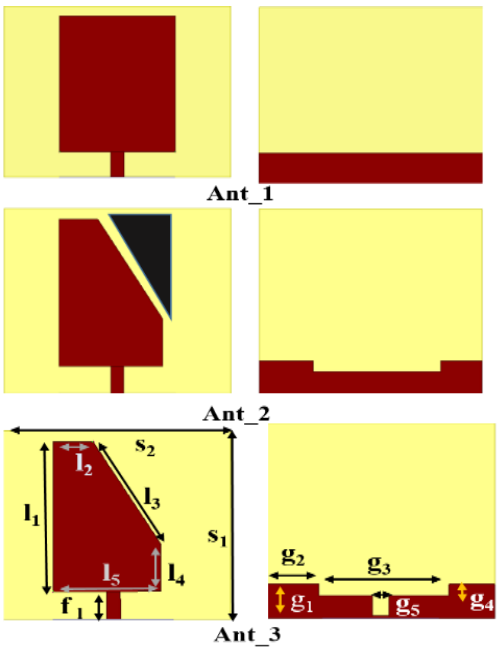

Figure 1. Single antenna evolution and geometry of optimized single monopole antenna [l_1=27, l_2=6, l_3=22, l_4=8.6, l_5=16, f_1=5, s_1=35, s_2=34, g_1=6, g_2=8.5, g_3=20, g_4=2, g_5=2.5] (All values are in mm.)

The antenna is affixed to a substrate of Rogers R03003 with a dielectric constant value (ε_r) of 3.2. Here is a rectangular slot etched from the ground planes, which is shown as Ant._2, which notably improves the antenna's bandwidth, gain, and performance, and a refined single monopole antenna featuring a T-slot etched into the ground plane, referred to as the modified ground of the optimized antenna (Ant._3), as depicted in Figure 1.

2.2 2-Port MIMO antenna configuration

Figure 2 depicts the progression of the incremental evolution of the 2-element MIMO antenna. The overall dimension of this antenna is 34×64.5×1.6 mm^3. The symmetrical antennas are printed vertically and share a common ground, as shown in Figure 2(a). The conventional space between the antennas indicates the space diversity of the side-by-side antennas (G=43 mm) at 3.52 GHz, which is calculated by using Eq. (1) [7, 8, 31]. The center-to-center distance is adjusted from 31.5 mm to 33.5 mm, showcasing space diversity. To boost the antenna performance, a parametric study optimizes 'G' to 32.5 mm for a more compact design with enhanced diversity parameters.

$$G = \frac{\lambda_{max}}{2}$$
$$\lambda_{max} = \frac{c}{f} = 300/3.52 = 85.2271\text{mm} \quad (1)$$
$$\frac{\lambda_{max}}{2} = \frac{85.2271}{2} = 42.61\text{mm}$$

Eq. (2) [7, 8, 30] is used to calculate the isolation between two antennas. The isolation determines the degree of interference between the antennas and can affect the overall system's performance levels. For instance, the coupling coefficient (S_{ij}) is a measure of the coupling between two antennas (i & j).

$$Isolation = 20log_{10}\left(\frac{1}{\sqrt{\left(1-|S_{ij}|^2\right)}}\right) \quad (2)$$
$$Isolation = -20log_{10}(S_{ij})$$
$$Isolation = -20log_{10}(0.0794) = 22\ dB$$

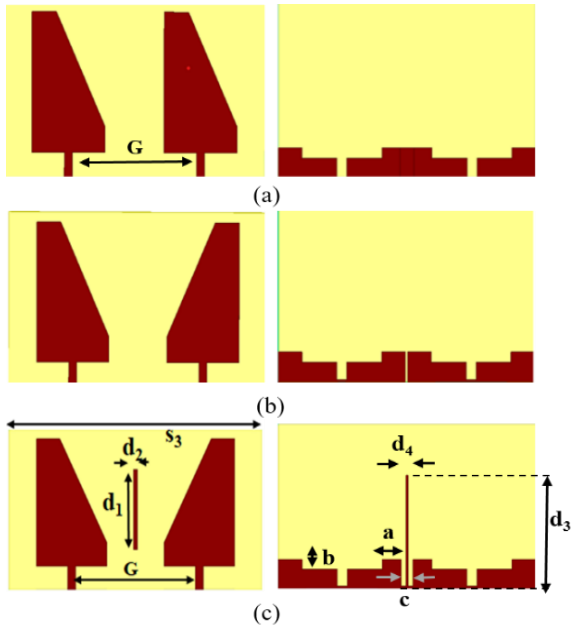

Figure 2. Geometry of the two-port MIMO antenna (a),(b),(c) evolutions of Ant.-a, Ant.-b, and Ant.-c [s_3=64.5, d_1=17, d_2=1, d_3=23, d_4=0.5, a=4.75, b=4.5, c=3] (All values are in mm.)

In addition, the T-shaped slot etching from the ground plane modifies the current distribution in the antennas and mitigates

coupling. Figure 2(b) depicts the second element's mirrored image of the first element, which diminishes the antenna's. The dimensions remain the same, and a centre slot is incorporated in the middle of the common ground. Furthermore, by including a vertical grounding branch element connected to the ground, it can generate a new coupling current and further mitigate the coupling of the Ant._c. Strategically, the optimized decoupling element has a length (d_1) of 17mm (ranging from 15 to 21 mm) and a width (d_2) of 1mm (ranging from 0.5 to 2.5 mm). In the rear view, the Ant._c grounding branch length (d_3) is optimized at 23mm (ranging from 21 to 25 mm) with a width (d_4) of 0.5mm. This design alters the current pathway within the ground plane and the patch, which mitigates the interference between the antennas and enhances the isolation compared to the previous design.

2.3 The proposed 4-port MIMO (2×2 configuration) antenna design

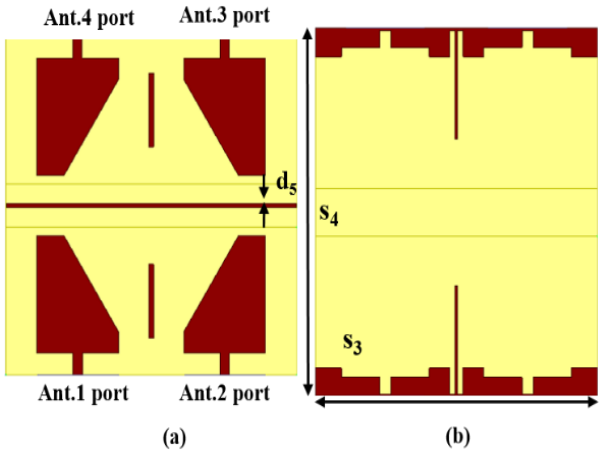

Figure 3. The suggested 4-port (2×2) MIMO antenna showcases (a) the front view and (b) the rear view. The provided parameters consist of [d_5=1, S_3=64.5, S_4=78], with all measurements in mm

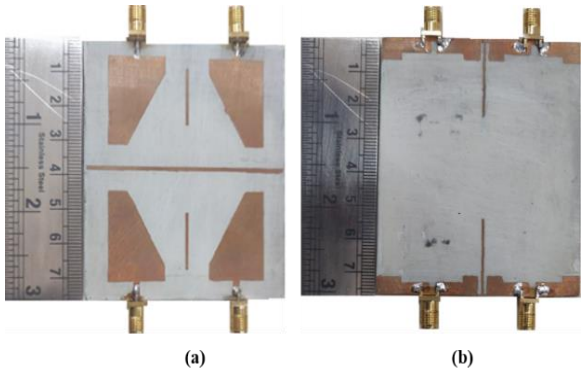

Figure 4. The fabricated snapshots of a 4-port MIMO antenna with SMA connectors are presented in (a) the top view and (b) the rear view

The proposed design is illustrated in Figure 3. In this method, two 2-element MIMO antennas are placed orthogonally and extended. Another decoupling stub is then placed strategically between the two 2-element MIMO antennas, as shown in Figure 3(a). The optimized width (d_5) is 1mm (ranging from 0.25 to 1.25mm) and length 64mm, which reduces the S_{21} and enhances the planned antenna performance for real-time scenarios. The final optimized dimension of the suggested 4-port MIMO antenna for this design is 78×64.5×1.6 mm^3 and adds the substrate between two antenna pairs with another decoupling element. As a result, the suggested modified ground and stub can efficiently reduce S_{21} between the antenna ports to achieve the desired diversity performance in the 5G MIMO antenna design.

Figure 4 depicts the fabricated prototypes of the proposed antennas with 50Ω SMA connectors.

3. RESULTS AND DISCUSSION

Figure 5 depicts the testing setup of the designed MIMO antenna using an Anritsu VNA MS2037C/2 vector network analyzer utilized to validate the operational capabilities. In this setup, Port 1 is excited while the other ports are set with 50-ohm matching. Figure 5(a) shows the measuring setup of S_{xx} in dB and Figure 5(b) shows the measurement of S_{xy} in dB.

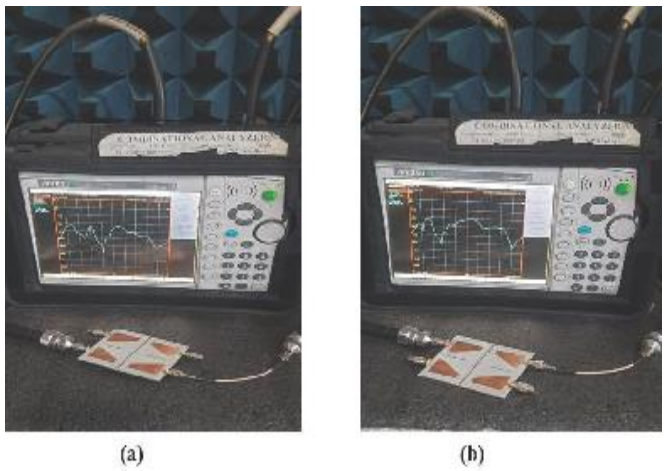

Figure 5. Anritsu VNA MS2037C/2 setup for testing a proposed 4-port MIMO antenna (a) measuring S_{xx} in dB and (b) measuring S_{xy} in dB

In Figure 6(a), the results of S_{11} illustrate the step-by-step evolution of single monopole antennas (Ant.-1,2, and 3). Ant.-3 changes its frequency response as it evolves and gets better, which leads to better power transfer at the receiver end and greater impedance matching with S_{11}<-10 dB. This optimization achieves a bandwidth of 2.8–4.2 GHz, reaching -28.5 dB at 3.6 GHz. Figure 6(b), on the other hand, shows a separate parametric analysis of a single antenna that has been optimized and has a ground plane length of g_2=g_4=8.5mm (between 8 and 9mm). It covers the same required band with superior impedance matching, with S_{11} measuring -41.5 dB at 3.6 GHz.

The simulation results of the 2-identical element arranged in a linear manner (MIMO configuration) with varying gap lengths (G) are depicted in Figure 7(a). The observed S-parameters show G ranging from 31.5 to 35mm, with the maximum gap at 35 mm, indicating increased signal reflection. A notable improvement is achieved at 32.5 mm; it achieves 1.39 GHz in the frequency spectrum of 2.81–4.2 GHz. Figure 7(b) visually presents the S_{21}values corresponding to various isolation techniques explored in this study, encompassing symmetry, mirroring techniques (-12.3 dB to -15.7 dB), and optimized decoupling employing grounding branch elements of modified ground (-15.7 dB to -22 dB).

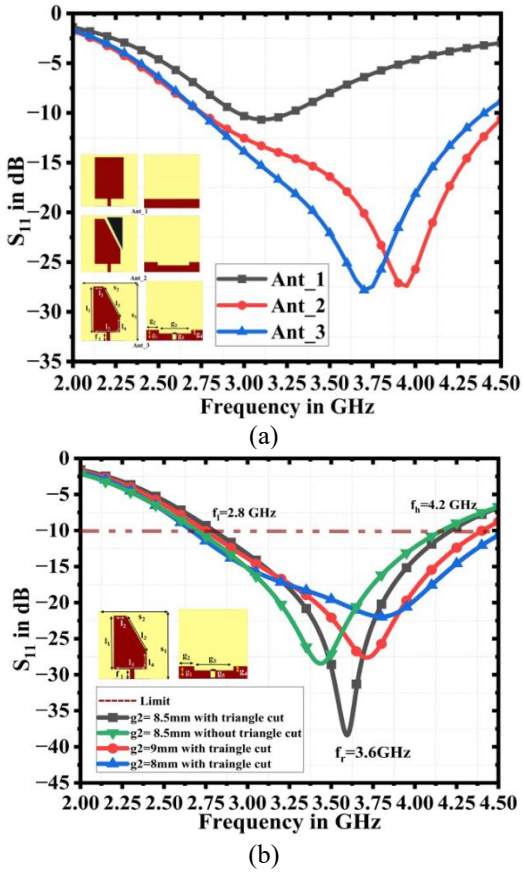

Figure 6. Simulated monopole antenna results of S_{11}(dB). (a) Evolution of antenna corresponding results. (b) various g_2 values with and without triangle cut

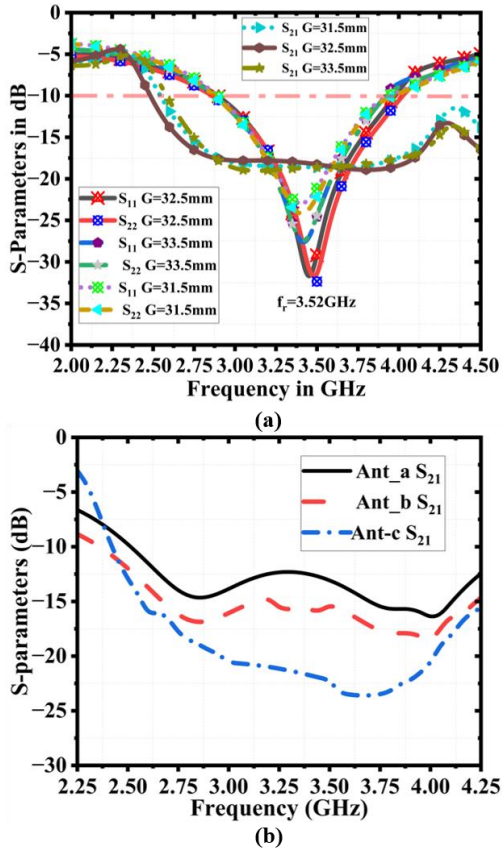

Figure 7. Simulation outcomes of a 2×1 MIMO antenna. (a) Simulated results S_{xx} of the gap (G) between the antennas. (b) Evolution S_{21} results of the 2-port MIMO configuration

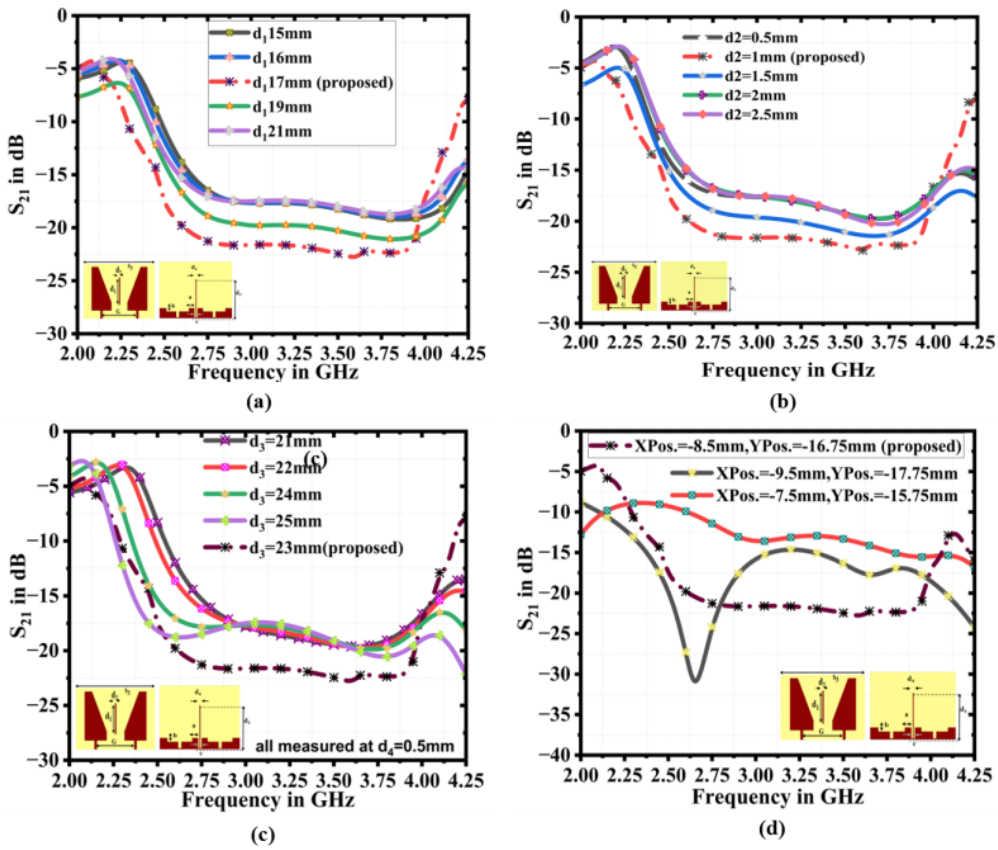

Figure 8. Simulated parameterized S_{21} outcomes for a 2×1 MIMO antenna. (a) Different lengths (d_1). (b) Different widths (d_2). (c) Various lengths (d_3). (d) Different positions of the decoupling element (XPos. and YPos.)

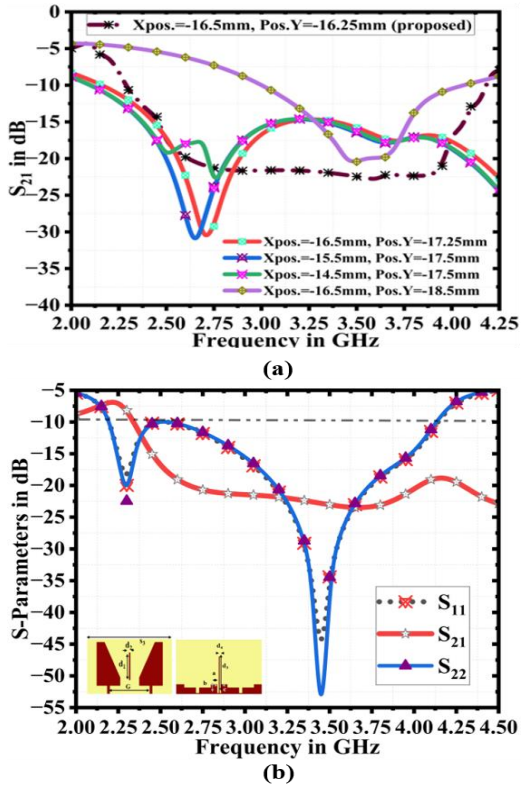

Figure 9. The simulation results for a 2×1 MIMO antenna. (a) Results depicting varied positions of the grounding branch. (b) S-parameter outcomes for the optimized 2×1 MIMO antenna

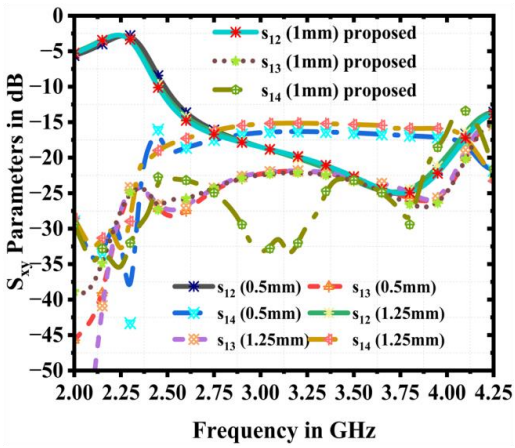

Figure 10. The S_{xy} (dB) characteristics of the suggested four-port MIMO antenna based on a simulated d_5 parametric analysis

Figure 8 shows a different set of parametric analyses that focus on the isolation techniques that were used, with a focus on the decoupling stubs (DS) and grounding branch with modified ground. The length of the DS, denoted as d_1, varies from 15mm to 21mm, leading to S_{21} values ranging from -17 dB to -22.5 dB. Following optimization, d_1 is set at 17mm, achieving S_{21} of -17 dB, as depicted in Figure 8(a). The width of the DS, labeled by d_2 , ranges from 0.5 to 2.5mm, resulting in S_{21} values from -16.5 dB to -22 dB. After optimization, d_2 is determined to be 1mm, resulting in an S_{21} of -22 dB, as depicted in Figure 8(b).

In Figure 8(c), the width (d_4) of the grounding branch is fixed at 0.5mm. Meanwhile, the length, denoted as d_3, varies from 21mm to 25mm, yielding S_{21} values ranging from -16.5 dB to -22.5 dB. Following optimization, d_3 is set at 23mm, achieving an S_{21} of -22.5 dB. The effectiveness of isolation depends not only on the dimensions but also on the positioning of the DS and the modified ground. Figure 8(d) displays the varying positions of the DS, ranging from 8.5mm to 17.75mm, resulting in S_{21} values from -11 to -22 dB. The fixed coordinates for XPos. and YPos. are set at -8.5mm and -16.75mm, respectively, measured from the center of the ground plane. Figure 9(a) illustrates the positioning of the grounding branch in the middle of the modified ground, adjusting XPos. and YPos. in a range from 16.25mm to 18.5mm. After optimization, the ideal XPos. and YPos. are determined to be 16.25mm each, achieving superior performance with low coupling and a remarkable S_{21} of below -22 dB.

The optimization of the feed ground cut (c) at 3mm is based on the simulation results from the grounding branch, as depicted in Figure 9(b). Based on these findings, the best MIMO antenna (2×1) with a 2 GHz bandwidth can get an impedance value of -54.5 dB at 3.52 GHz and an S_{21} value below -23.25 dB.

The suggested four-port MIMO configuration incorporates an additional decoupling element (DE) positioned in the middle of the straight lines connecting the two-element MIMO pairs. The optimized DE length is 64mm, and the width d_5 varies from 0.5 to 1.25mm. The simulated S_{xy} results are depicted in Figure 10, showcasing different S_{xy} levels below -15 dB from one antenna to the rest of the antennas. After optimization, d_5 is set at 1mm, achieving improved S_{21} of -22 dB, S_{31} of -26 dB, and S_{41} of -31 dB.

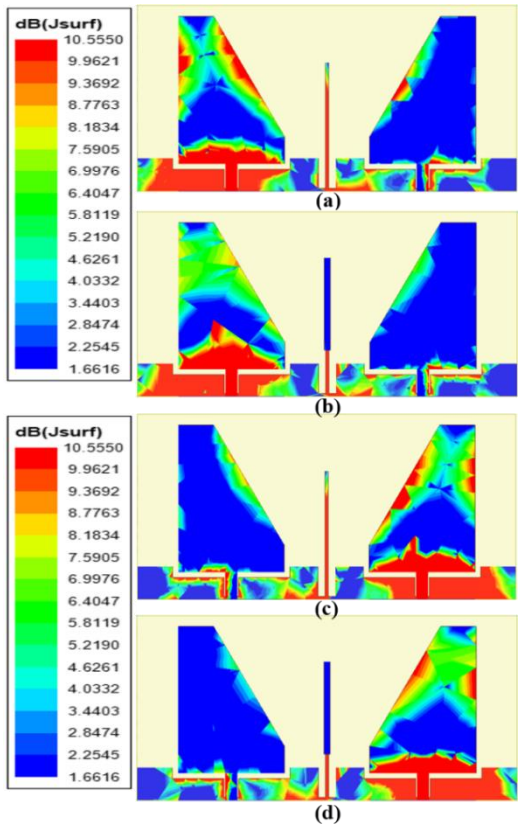

Figure 11. Distribution of simulated electric field at the front-line antenna of a 2×1 MIM0 antenna at 3.52 GHz. (a) Port 1 excited with and without coupling element. (b) Port 2 excited with and without coupling element

The progressive use of all isolation techniques and strategic placement (XPos., YPos.) of the decoupling element dimensions (d_1, d_2, d_3, d_4, and d_5) in the design reduces the electric field that gets coupled from one element to another, resulting in an enhancement of the isolation (S_{21}). Figure 11 depicts the distribution of the electric field within the 2-element configuration at 3.52 GHz. It showcases the impact of a decoupling element on the enhancement of the isolation techniques. As depicted in these results, more electric fields get coupled to the neighbouring element when no decoupling elements are present. A reduction in the electric field that gets correlated from one element to another is achieved by strategically placing the decoupling elements in the design, which mitigates the coupling (S_{21}) of one antenna to another.

Furthermore, the isolation varies when decoupling elements are introduced between the antennas of the four-port MIMO configuration. In this examination, one port (the antenna source) is excited while the remaining ports are terminated with 50 ohms. In Figure 12, when the first port is activated without the decoupling elements, the antenna elements 2-4 exhibit higher coupling. Upon the incorporation of the decoupling elements, the coupling is diminished as these elements block the coupling current between the antennas. Similar scenarios unfold when the remaining ports are activated.

A similar improvement in the coupled electric field is achieved over the complete N77, N78, and N48 frequency bands with the use of the decoupling elements. The experimental results are examined and contrasted with the actual simulation results of the suggested four-port MIMO (2×2) configuration. The next sections provide a detailed study of the comparison between the experimental and generated results. For brevity, this paper the discusses results based on the 2-way antenna, and the remaining antennas are symmetrically matched. The simulation and measurement parameter values for reflection coefficient, transmission coefficient, TARC, ECC, DG, CCL, gain and radiation pattern, multiplexing efficiency, and MEG for different configurations can be observed in Figures 13-20. The comprehensive outcomes of the final designed four-port MIMO configuration antenna are elaborated as follows.

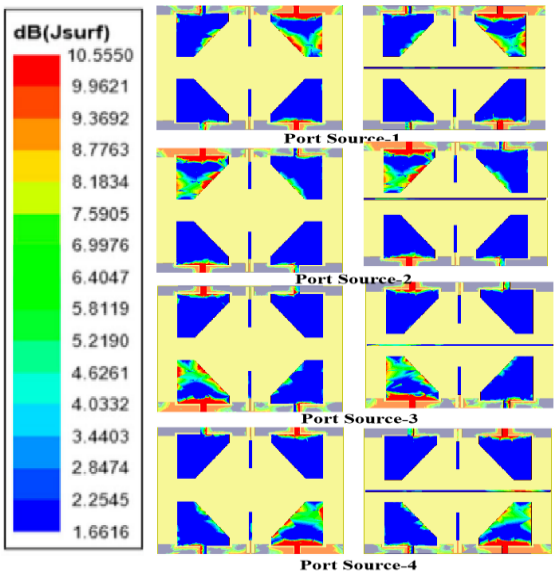

Figure 12. Simulated surface current density distribution at the front line antenna of a 4-element with and without decoupling element (DE)3 MIM0 antenna at 3.52GHz

3.1 S-parameters (S_{ii} and S_{ij})

A comparison plot of the simulation and measurement S_{ii}-parameters results for the four-port MIMO design is shown in Figure 13(a).

This plot facilitates a visual assessment of the agreement or variance between the simulated and experimentally measured values of the S-parameters of the system. S_{ii} is at -35 dB at 3.52 GHZ; it indicates a low level of reflection, which is desirable for efficient signal transmissions and suitable impedance matching across the bandwidth. The S_{ii} curve of the suggested 4-port MIMO antenna achieved a bandwidth (S_{ii} <- 10 dB) of 1.50 GHz (ranging from 2.7 GHz–4.2 GHz). The observed variation could be the result of fabrication tolerance. It is suitable for the FR-1 sub-bands denoted as n77 (TDD 3.300–4.200 GHz), n78 (TDD 3.300–3.800 GHz), and n48 (TDD 3.550–3.700 GHz) bands of 5G-NR applications. In Figure 13(b), the transmission coefficient measures the amount of energy transmitted by the antenna to the receiver. Figure 13(b) compares the actual results with the expected ones. At the lower band, S_{21} is -21 dB; at the upper band, it is -25 dB; and the overall band attains -22 dB. The recommended 4-port MIMO antenna achieves higher isolation.

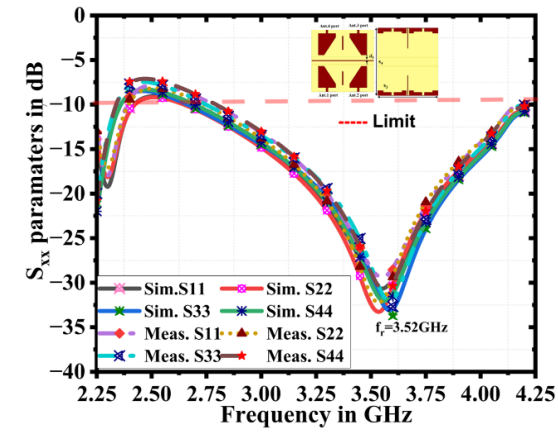

(a)

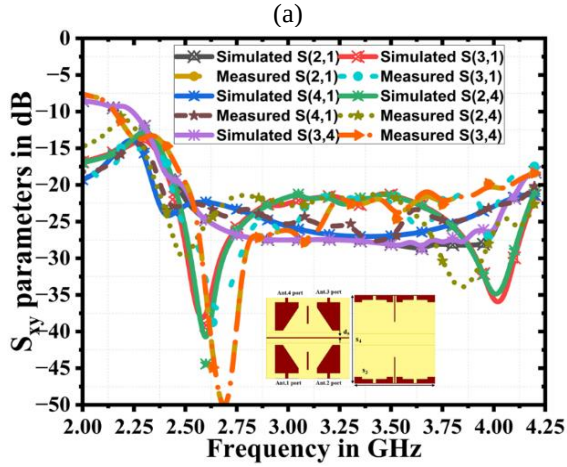

(b)

Figure 13. Comparison of the 4-port MIMO antenna simulation and experiment results. (a) S_{xx} parameters. (B) S_{xy} parameters

3.2 Diversity parameters

3.2.1 Total active reflection coefficient (TARC)

The measure of the TARC between two ports is calculated by Eq. (3) [22, 30-32]. For brevity, this paper considers a 2-

way TARC and the other two ports to be matched in a 4-port MIMO antenna due to its identical structure.

$$TARC\ (\Gamma) = \sqrt{\frac{|S_{ii} + S_{ij}|^2 + |S_{ji} + S_{jj}|^2}{2}} \quad (3)$$

The actual and determined TARC results, shown in Figure 14, are both <-10 dB of the targeted band. The TARC parameter is evaluated using the relation, which indicates a good reflection and signal low loss level, ideal for efficient signal transfers.

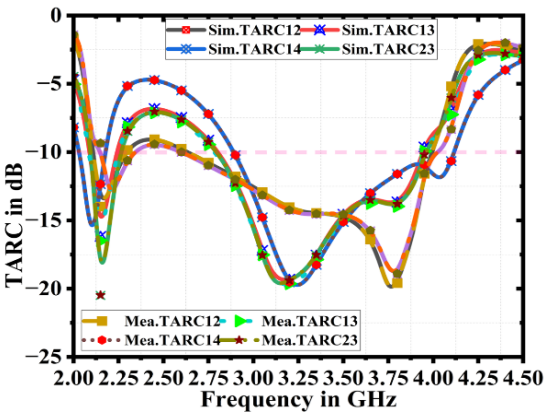

Figure 14. Simulated and measured TARC (dB) results vs. frequency (GHz)

3.2.2 Envelope correlation coefficient (ECC)

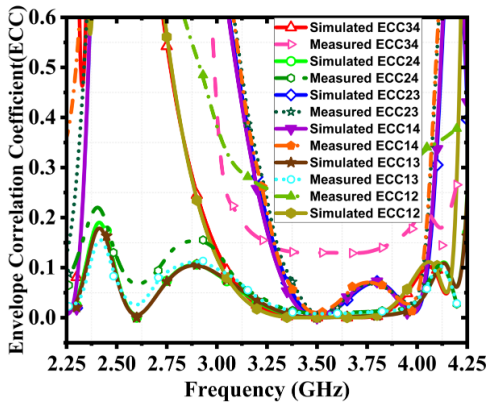

(a)

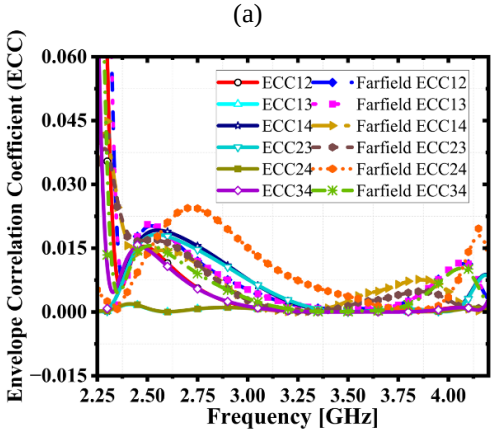

(b)

Figure 15. Comparative ECC results. (a) simulation vs. measurement results based on S-parameters. (b) simulation results based on far-field and S-parameters

Eq. (4) [22, 31] calculates the ECC according to scattering parameter values across various ports, and Eq. (5) [22, 31, 32]. computes the radiation pattern. The ECC_{24} value is 0.001, indicating a relatively lower value. Similarly, the ECC_{12} value is measured to be 0.015. When considering the overall average ECC for all ports, it amounts to 0.0078. On the other hand, a contrast of the observed and modeled results is shown in Figure 15(a), explicitly highlighting the ECC values. In this case, the ECC_{13} value is 0.001, indicating a low value. The ECC_{34} value is 0.35. This is significantly elevated and quantifies the degree of correlation between the signal envelopes acquired by the system's several antenna ports.

$$ECC = \frac{\left|S_{ii}^{*}S_{ij} + S_{ji}^{*}S_{ji}\right|^2}{\left(1 - |S_{ii}|^2 - |S_{ji}|^2\right)\left(1 - |S_{jj}|^2 - |S_{ij}|^2\right)} \quad (4)$$

$$ECC = \frac{\left|\iint_{4\pi}[E_i(\theta,\emptyset) * E_j(\theta,\emptyset)d\Omega\right|^2}{\left|\iint_{4\pi}|E_i(\theta,\emptyset)|^2\right|d\Omega * \left|\iint_{4\pi}\left|E_j(\theta,\emptyset)\right|^2\right| d\Omega} \quad (5)$$

A lower ECC value indicates better diversity performance. In the mentioned work, an ECC value of 0.0078 is achieved, significantly below the acceptable threshold of 0.5. The ECC values obtained from the S-parameters and the far-field radiation patterns are displayed in Figure 15 (b). ECC pertains to comparing the radiation patterns and scattering properties between each pair of the suggested antenna ports.

3.2.3 Diversity gain (DG)

Eq. (6) [22, 31, 32] determines the DG based on ECC characteristics between different ports. Figure 16 shows the diversity gain of the final-designed antenna. The obtained values indicate a significant improvement in signal quality and performance.

$$DG = 10 * \sqrt{(1 - ECC^2)} \quad (6)$$

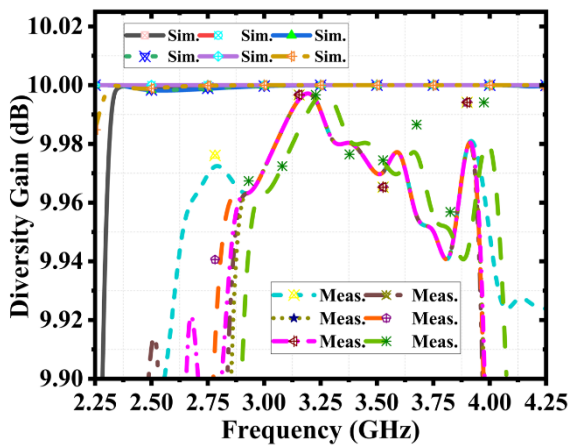

Figure 16. Simulated and measured results of the DG (dB)

For this scenario, the minimum D.G. value is 9.94 dB, while the higher value is 9.98 dB. Furthermore, the overall DG is 9.96 dB. These values indicate that the system is capable of significantly enhancing signal quality through the use of multiple antennas.

3.2.4 Channel capacity loss (CCL)

Figure 17 shows the simulated CCl results for the suggested

four-port MIMO configuration based on the s-parameters set to different ports. With ports 3-4, it attains a data rate of 0.24 bits/s/Hz, while the remaining ports reach a rate of 0.05 bps/Hz. Eq. (7) [22, 33] determines the CCL based on radiation and S-parameter characteristics between different ports. CCL indicates a relatively low level of correlation, which means that the system can achieve good diversity and minimize interference from other signals.

$$CCL = -log_2 \det(A) \quad (7)$$

where, $A = \begin{bmatrix} a_{11} & a_{12} \\ a_{21} & a_{22} \end{bmatrix}$, $a_{ii} = 1 - (|S_{ii}|^2 + |S_{ij}|^2)$, $a_{ij} = (S_{ij}^* S_{ij} + S_{ji} S_{jj}^*)$, for I, j=1 or 2.

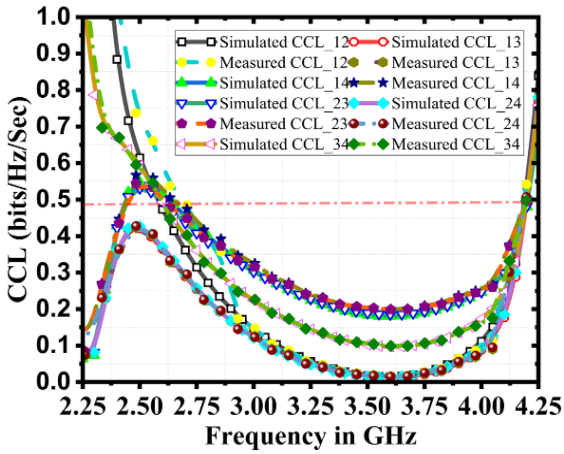

Figure 17. Results of measurements and simulations for the CCL (bps/Hz)

3.2.5 Mean effective gain (MEG)

MEG is calculated using Eq. (8) [34]. The channel is assumed to be Rayleigh with identical polarization densities for improved channel characteristics and diversity performance. The criteria of K= MEG_i.-MEG_j. less than 3 dB are considered, and Figure 18 illustrates that the MEG is less than 0.01 dB, indicating a favorable outcome.

$$MEG_{i.} = 0.50\eta_{i.,}rad = 0.50[1 - \sum_{j.=1}^{N} |S_{i,j}|^2] \quad (8)$$

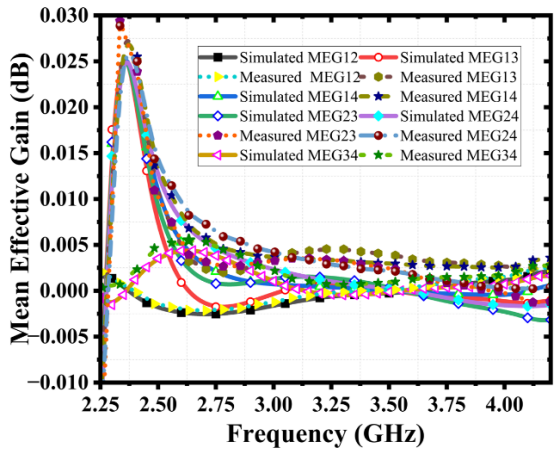

Figure 18. Comparative results of measurements and simulations for the MEG (dB)

3.2.6 Gain and radiation efficiency, radiation pattern

Figure 19 shows the suggested four-port MIMO antenna's measurement and simulation results for the gain, as well as a plot of the radiation efficiency against frequency. The results indicate a consistent variation, showcasing stable gain within the range of approximately 3.5 to 4.7 dBi and radiation efficiency spanning from 97% to 98.85%. Notably, these observed values are slightly lower than those predicted by the simulation. It is better for MIMO antennas to work in certain 5G frequency bands because they can send and receive more information without any problems. The suggested antenna design achieved a high radiating efficiency of over 98.85%.

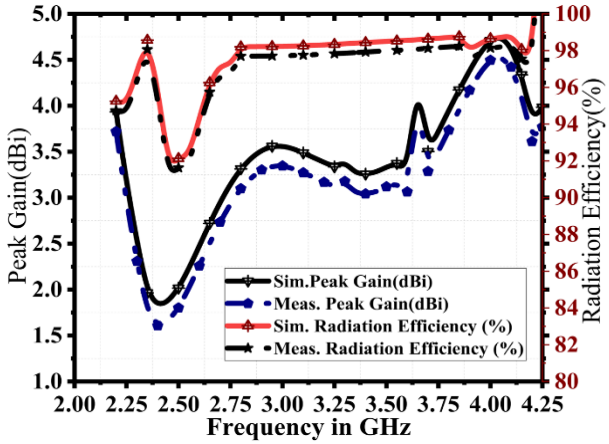

Figure 19. Simulated versus measured results. (a) peak gain (dBi) versus frequency. (b) simulated radiation efficiency vs. frequency results

The radiation patterns of a two-dimensional (2D) MIMO antenna are shown in Figure 20. It shows both cross-polarization and co-polarization effects. The radiation characteristics are evaluated at 3.52 GHz and analyzed in both the YZ-plane (φ=0°) and the XY-plane (φ=90°) as the E and H-planes. Noteworthy enhancements were detected at these resonant frequencies, indicating reduced cross-polarizatio thereby positively influencing the overall antenna performance. While monitoring the pattern of power radiated from one port, the rest of the ports are matched. Table 1 presents the state-of-the-art advancements in the proposed antenna. It has conducted a comparative analysis to evaluate the proposed antenna against existing research. The proposed MIMO antenna achieves high isolation (S_{21}), 98% efficiency, and demonstrates good diversity performance.

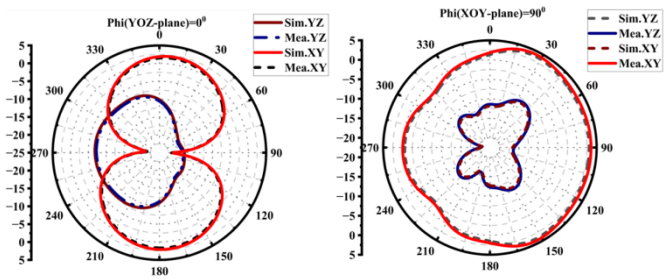

Figure 20. Evaluating and contrasting the radiation patterns for antenna 1 across the YOZ and XOZ planes

Table 1. State-of-the-art analysis to compare the suggested antenna with the existing research

Ref.	Size (mm^2)	S_{21} (dB)	ECC	D.G. (dB)	TARC (dB)	M.E.G (dB)	CCL (bps/Hz)	Efficiency (%)	Gain (dBi)	No. of Ports	Year
[31]	133 × 133	16.5	0.001	-	-	-	-	84	5.2-6.8	4	2020
[35]	60 × 60	19	0.12	-	-	-	0.349	-	-	4	2020
[1]	180 × 180	14	0.01	-	-	-7.96	-	70	0.05, 4.4, 6.9, 5	4	2021
[36]	70 × 145	20	0.5	-	-	-	-	70	4-5.5	4	2021
[37]	100 × 100	15	0.03	-	-	-5	-	80	6.1-7.5	4	2021
[38]	90 × 90	25	0.5	9.8	-	-	21	74	4	4	2022
[39]	55 × 55	15	0.017	-	-	-	-	68	4	4	2022
[40]	120 × 60	15	0.12	9.9	-	-	-	76-91	-	4	2022
[41]	65 × 60	15	0.13	9	-12.5	1.0057	-	-	-	4	2022
[42]	72 × 72	15	0.005	10	-10	-3	0.05	72	2.5	4 & 8	2023
P.A.	**64.5 × 78**	**22**	**0.00789**	**9.96**	**-15**	**0.05**	**0.08**	**98**	**4.4**	**4**	**present**

4. CONCLUSIONS

The two-element antenna and four-element (2×2 configuration) MIMO antennas in this work are designed to make 5G-NR (n77/n78/n48 bands) communication systems more efficient, improve diversity, and improve isolation. The suggested 4-port MIMO antenna has an S11 of -35 dB (2.7–4.2 GHz), an isolation s21 of -22 dB, a TARC of -10 dB, an ECC level of 0.0078, and a DG of 9.96 dB. These results show that the system can achieve good diversity performance and better performance levels. Its low CCL level of 0.05 bps/Hz shows that it can handle other signals without much trouble and has a good radiation pattern in the co- and cross-polarization, giving it a gain of about 4.4 dBi. One potential area of future development is using advanced materials and fabrication techniques to further optimize these antenna configurations' performance. For example, using metamaterials or other novel materials can help improve the antenna diversity parameters. Another area of future development is the integration of these antenna configurations with other wireless technologies such as 5G, IoT, and satellite communication systems. Furthermore, there is a prospect for additional optimization of the antenna configurations using machine learning (ML) and artificial intelligence (AI) methodologies.

ACKNOWLEDGMENT

I wish to extend my sincere appreciation to Dr. N. V. Rajasekhar, my mentor, for his invaluable guidance, expertise, and unwavering support during the entire duration of this research. The direction and quality of this essay were greatly influenced by Dr. Rajasekhar's vast expertise, smart inputs, and persistent support. Additionally, I express my gratitude to VIT-AP University for the comprehensive provision of resources and facilities throughout the course of my work.

REFERENCES

[1] Jha, K.R., Jibran, Z.P., Singh, C., Sharma, S.K. (2021). 4-port MIMO antenna using common radiator on a flexible substrate for sub-1GHz, sub-6GHz 5G NR, and Wi-Fi 6 applications. IEEE Open Journal of Antennas and Propagation, 2: 689-701. https://doi.org/10.1109/OJAP.2021.3083932

[2] Kumar, S., Dixit, A.S., Malekar, R.R., Raut, H.D., Shevada, L.K. (2020). Fifth generation antennas: A comprehensive review of design and performance enhancement techniques. IEEE Access, 8: 163568-163593. https://doi.org/10.1109/ACCESS.2020.3020952

[3] Parkvall, S., Dahlman, E., Furuskar, A., Frenne, M. (2017). NR: The new 5G radio access technology. IEEE Communications Standards Magazine, 1(4): 24-30. https://doi.org/10.1109/MCOMSTD.2017.1700042

[4] Manumula, S., Rajasekhar, N.V. (2023). Design of compact MIMO antenna for 5G Applications. In 2023 3rd International conference on Artificial Intelligence and Signal Processing (AISP), VIJAYAWADA, India, pp. 1-5. https://doi.org/10.1109/AISP57993.2023.10134970

[5] Sharma, M., Awasthi, Y.K., Singh, H. (2017). Design of compact planar triple band-notch monopole antenna for ultra-wideband applications. Wireless Personal Communications, 97: 3531-3545. https://doi.org/10.1007/s11277-017-4684-3

[6] Sharma, M., Kumar, R., Kaur, P., Dhasarathan, V., Nguyen, T.K. (2022). Design and analysis of on-demand reconfigurable WiMAX/WLAN high isolation 2×2 MIMO antenna oriented adjacent/orthogonally for imaging applications in UWB-X band. International Journal of RF and Microwave Computer-Aided Engineering, 32(1): e22928. https://doi.org/10.1002/mmce.22928

[7] Jayant, S., Srivastava, G. (2022). Close-packed quad-element triple-band-notched UWB MIMO antenna with upgrading capability. IEEE Transactions on Antennas and Propagation, 71(1): 353-360. https://doi.org/10.1109/TAP.2022.3222768

[8] Srinubabu, M., Rajasekhar, N.V. (2024). Enhancing diversity and isolation performance for a four-port MIMO antenna in FR-1 5G frequency bands. IETE Journal of Research, 1-16. https://doi.org/10.1080/03772063.2024.2324025

[9] Srinubabu, M., Rajasekhar, N.V. (2024). A compact and efficiently designed two-port MIMO antenna for N78/48 5G applications. Heliyon, 10(7): E28981. https://doi.org/10.1016/j.heliyon.2024.e28981

[10] Molins-Benlliure, J., Cabedo-Fabrés, M., Antonino-Daviu, E., Ferrando-Bataller, M. (2022). sector unit-cell methodology for the design of Sub-6 GHz 5G MIMO antennas. IEEE Access, 10: 100824-100836. https://doi.org/10.1109/ACCESS.2022.3207163

[11] Sufian, M.A., Hussain, N., Askari, H., Park, S.G., Shin,

K.S., Kim, N. (2021). Isolation enhancement of a metasurface-based MIMO antenna using slots and shorting pins. IEEE Access, 9: 73533-73543. https://doi.org/10.1109/ACCESS.2021.3079965

[12] Kumari, P., Gangwar, R.K., Chaudhary, R.K. (2022). An aperture-coupled stepped dielectric resonator UWB MIMO antenna with AMC. IEEE Antennas and Wireless Propagation Letters, 21(10): 2040-2044. https://doi.org/10.1109/LAWP.2022.3189694

[13] El-Din, M.S., Shams, S.I., Allam, A.M.M.A., Gaafar, A., Elhennawy, H.M., Sree, M.F.A. (2022). SIGW based MIMO antenna for satellite down-link applications. IEEE Access, 10: 35965-35976. https://doi.org/10.1109/ACCESS.2022.3160473

[14] Zhang, Y., Shen, S., Han, Z., Chiu, C.Y., Murch, R. (2021). Compact MIMO systems utilizing a pixelated surface: Capacity maximization. IEEE Transactions on Vehicular Technology, 70(9): 8453-8467. https://doi.org/10.1109/TVT.2021.3101687

[15] Sufian, M.A., Hussain, N., Abbas, A., Lee, J., Park, S.G., Kim, N. (2022). Mutual coupling reduction of a circularly polarized MIMO antenna using parasitic elements and DGS for V2X communications. IEEE Access, 10: 56388-56400. https://doi.org/10.1109/ACCESS.2022.3177886

[16] Yuan, X.T., Chen, Z., Gu, T., Yuan, T. (2021). A wideband PIFA-pair-based MIMO antenna for 5G smartphones. IEEE Antennas and Wireless Propagation Letters, 20(3): 371-375. https://doi.org/10.1109/LAWP.2021.3050337

[17] Tang, H., Bulger, C. J., Rovere, T., Zheng, B., An, S., Li, H., Dong, Y.X., Haerinia, M., Fowler, C., Gonya, S., Guo, W., Zhang, H. (2022). A low-profile flexible dual-band antenna with quasi-isotropic radiation patterns for MIMO system on UAVs. IEEE Antennas and Wireless Propagation Letters, 22(1): 49-53. https://doi.org/10.1109/LAWP.2022.3201492

[18] Addepalli, T., Babu Kamili, J., Kumar Bandi, K., Nella, A., Sharma, M. (2022). Lotus flower-shaped 4/8-element MIMO antenna for 5G n77 and n78 band applications. Journal of Electromagnetic Waves and Applications, 36(10): 1404-1422. https://doi.org/10.1080/09205071.2022.2028683

[19] Liu, L., Cheung, S.W., Yuk, T.I. (2015). Compact MIMO antenna for portable UWB applications with band-notched characteristic. IEEE Transactions on Antennas and Propagation, 63(5): 1917-1924. https://doi.org/10.1109/TAP.2015.2406892

[20] Xu, Y., Dong, Y., Wen, S., Wang, H. (2021). Vertically polarized quasi-Yagi MIMO antenna for 5G N78 band application. IEEE Access, 9: 7836-7844. https://doi.org/10.1109/ACCESS.2020.3049058

[21] Kulkarni, J., Garner, B., Li, Y. (2023). A dual CP quad-port MIMO antenna with reduced mutual coupling for X-band application. IEEE Antennas and Wireless Propagation Letters, 22(9): 2085-2089. https://doi.org/10.1109/LAWP.2023.3275530

[22] Moses, A.T.Z., Moses, N., Janapala, D.K. (2022). An electrically small 4-port self-decoupled MIMO antenna pairs operating in n78 5G NR band for smartphone applications. AEU-International Journal of Electronics and Communications, 145: 154082. https://doi.org/10.1016/j.aeue.2021.154082

[23] Satam, V., Nema, S. (2018). Two element compact UWB diversity antenna with combination of DGS and parasitic elements. Wireless Personal Communications, 98: 2901-2911. https://doi.org/10.1007/s11277-017-5006-5

[24] Hussain, M., Awan, W.A., Ali, E.M., Alzaidi, M.S., Alsharef, M., Elkamchouchi, D.H., Alzahrani, A., Sree, M.F.A. (2022). Isolation improvement of parasitic element-loaded dual-band MIMO antenna for mm-wave applications. Micromachines, 13(11): 1918. https://doi.org/10.3390/mi13111918

[25] Zhang, S., Pedersen, G.F. (2015). Mutual coupling reduction for UWB MIMO antennas with a wideband neutralization line. IEEE Antennas and Wireless Propagation Letters, 15: 166-169. https://doi.org/10.1109/LAWP.2015.2435992

[26] Urimubenshi, F., Konditi, D.B., de Dieu Iyakaremye, J., Mpele, P.M., Munyaneza, A. (2022). A novel approach for low mutual coupling and ultra-compact Two Port MIMO antenna development for UWB wireless application. Heliyon, 8(3): e09057. https://doi.org/10.1016/j.heliyon.2022.e09057

[27] Nadeem, I., Choi, D.Y. (2018). Study on mutual coupling reduction technique for MIMO antennas. IEEE Access, 7: 563-586. https://doi.org/10.1109/ACCESS.2018.2885558

[28] Zhang, X.X., Ren, A.D., Liu, Y. (2020). Decoupling methods of MIMO antenna arrays for 5G applications: A review. Frontiers of Information Technology & Electronic Engineering, 21(1): 62-71. https://doi.org/10.1631/FITEE.1900466

[29] Kumar, N., Kumar, P., Sharma, M. (2020). Reconfigurable antenna and performance optimization approach. Wireless Personal Communications, 112(4): 2187-2212. https://doi.org/10.1007/s11277-020-07145-0

[30] Addepalli, T., Anitha, V.R. (2020). A very compact and closely spaced circular shaped UWB MIMO antenna with improved isolation. AEU-International Journal of Electronics and Communications, 114: 153016. https://doi.org/10.1016/j.aeue.2019.153016

[31] Addepalli, T., Anitha, V.R. (2022). Parametric analysis of compact UWB-MIMO antenna with improved isolation using parasitic reflectors and protruded ground strips. Wireless Personal Communications, 1-17. https://doi.org/10.1007/s11277-021-09235-z

[32] Wong, K.L., Chen, J.Z., Li, W.Y. (2020). Four-port wideband annular-ring patch antenna generating four decoupled waves for 5G multi-input–multi-output access points. IEEE Transactions on Antennas and Propagation, 69(5): 2946-2951. https://doi.org/10.1109/TAP.2020.3025237

[33] Sree, G.N.J., Nelaturi, S. (2021). Design and experimental verification of fractal based MIMO antenna for lower sub 6-GHz 5G applications. AEU-International Journal of Electronics and Communications, 137: 153797. https://doi.org/10.1016/j.aeue.2021.153797

[34] Serghiou, D., Khalily, M., Singh, V., Araghi, A., Tafazolli, R. (2020). Sub-6 GHz dual-band 8× 8 MIMO antenna for 5G smartphones. IEEE Antennas and Wireless Propagation Letters, 19(9): 1546-1550. https://doi.org/10.1109/LAWP.2020.3008962

[35] Saxena, S., Kanaujia, B.K., Dwari, S., Kumar, S., Choi, H.C., Kim, K.W. (2020). Planar four-port dual circularly-polarized MIMO antenna for sub-6 GHz band. IEEE Access, 8: 90779-90791. https://doi.org/10.1109/ACCESS.2020.2993897

[36] Kulkarni, J., Alharbi, A. G., Desai, A., Sim, C.Y.D., Poddar, A. (2021). Design and analysis of wideband flexible self-isolating MIMO antennas for sub-6 GHz 5G and WLAN smartphone terminals. Electronics, 10(23): 3031. https://doi.org/10.3390/electronics10233031

[37] Wong, K.L., Ye, X.Q., Li, W.Y. (2022). Wideband four-port single-patch antenna based on the quasi-TM 1/2, 1/2 Mode for 5G MIMO access-point application. IEEE Access, 10: 9232-9240. https://doi.org/10.1109/ACCESS.2022.3144231

[38] Kulkarni, J., Sim, C.Y.D., Desai, A., Holdengreber, E., Talware, R., Deshpande, V., Nguyen, T.K. (2022). A compact four port ground-coupled CPWG-fed MIMO antenna for wireless applications. Arabian Journal for Science and Engineering, 47(11): 14087-14103. https://doi.org/10.1007/s13369-022-06620-z

[39] Kulkarni, N.P., Bahadure, N.B., Patil, P.D., Kulkarni, J.S. (2022). Flexible interconnected 4-port MIMO antenna for sub-6 GHz 5G and X band applications. AEU-International Journal of Electronics and Communications, 152: 154243. https://doi.org/10.1016/j.aeue.2022.154243

[40] Hussain, R., Abou-Khousa, M., Iqbal, N., Algarni, A., Alhuwaimel, S.I., Zerguine, A., Sharawi, M.S. (2022). A multiband shared aperture MIMO antenna for millimeter-wave and sub-6GHz 5G applications. Sensors, 22(5): 1808. https://doi.org/10.3390/s22051808

[41] Thangarasu, D., Palaniswamy, S.K., Thipparaju, R.R. (2023). Quad port multipolarized reconfigurable MIMO antenna for sub 6 GHz applications. International Journal of Antennas and Propagation, 2023: 8882866. https://doi.org/10.1155/2023/8882866

[42] Addepalli, T., Kumar, M.S., Jetti, C.R., Gollamudi, N.K., Kumar, B.K., Kulkarni, J. (2023). Fractal loaded, novel, and compact two-and eight-element high diversity MIMO antenna for 5G sub-6 GHz (N77/N78 and N79) and WLAN applications, verified with TCM analysis. Electronics, 12(4): 952. https://doi.org/10.3390/electronics12040952